Frequency-Domain Analysis of Coupled Nonuniform Transmission Lines Using Chebyshev Pseudo-Spatial Techniques

Guang-Wen Pan, *Member, IEEE,* Gregory J. Wunsch, and Barry K. Gilbert, *Senior Member, IEEE*

Abstract—**The analysis of nonuniform cross-section, lossy and coupled transmission lines is frequently necessary in the design and simulation of high speed microelectronics systems. This paper presents a method of performing such simulations on lossy lines of arbitrary cross section, under the quasi-TEM assumption. The technique incorporates a Chebyshev expansion in the frequency domain, and is one of the most suitable methods presently in existence for incorporation into computer aided design tools.**

I. Introduction

COUPLED LOSSY transmission lines with varying width and spacing are commonly found in the packaging of high-speed, high density digital electronics. Tapered transmission lines occur in nearly all single chip packages for high clock rate silicon ECL and Gallium Arsenide digital integrated circuits, in many printed circuit board layouts intended for such chips, at the edges of the newest metal-organic multichip modules (MCMs) where the internal leads fan out to accomodate the coarser geometries of hermetic packages and microwave connectors, and in similar locations in more conventional multilayer cofired ceramic substrates used by the analog microwave design community. At the frequencies and bandwidths for which the metal-organic and ceramic MCMs are being designed, it is absolutely necessary to be able to model the propagation of wavefronts through groups of tightly coupled, tapered stripline and/or microstrip interconnects, thereby to assure that waveform integrity will be preserved when the actual structures are fabricated and placed into service.

Previous analyses of the problem of modeling wavefront propagation along tapered transmission lines include the method of characters [1] and the time-domain perturbational method [2], among others. Recently, tapered transmission lines supporting non-TEM modes have been investigated [3]; tapered and dispersive lines terminated with nonlinear loads have also been described [4]. Palusinski [5] introduced a transient analysis of tapered lines by means of a Chebyshev expansion in the time domain under quasi-TEM assumptions. Although full-wave analyses are more general and rigorous, a quasi-TEM analysis can provide a good approximation in the frequency range below 5 GHz; nearly all of the present technology digital integrated circuits still operate within this bandwidth.

Of the previous methods, Palusinski's approach seems to be satisfactory for implementation as part of a computer aided analysis system. The simulation is suitable for arbitrary cross sections, handles multiple line systems and is computationally efficient. However, Palusinski's method was developed in the time domain; in this domain, the simulation of lossy lines is difficult, because skin effect resistance varies with frequency. The method presented here overcomes these difficulties by extending the method to the frequency domain. The advantages of a frequency domain approach over a time domain method lie in the following aspects: First, it can incorporate frequency parameters; second, it avoids the computation of recursive time steps, third, it avoids the computation of a state matrix e^A, thereby resulting in improved numerical efficiency and stability; finally, it is easier to integrate a frequency domain algorithm into CAD packages, since most transmission line networking programs conduct computations in the frequency domain [6]–[9]. The simulations performed with this method agree very well with previous examples of lossy multiple uniform line systems, and lossless non-uniform line systems as well.

II. Formulation

Two general geometric configurations of the problem to be solved by the new algorithm which will be presented below are depicted in Fig. 1, upper panel (Fig. 1U) for a single line and in Fig. 1, lower panel (Fig. 1L), for multiline cases, where the lines are assumed to be nonuniform and lossy. It is well known that the skin depth of conductors varies with the square root of frequency, provided that the metal thickness is much greater than the skin depth. The internal inductance of a conductor and the shunt conductance of imperfect dielectrics vary also with

Manuscript received October 31, 1991; revised March 25, 1992. This research was supported in part with funds from DARPA/MTO and DARPA/ESTO under contract N66001-80-C-0104 from the Naval Ocean Systems Center and contract F33615-86-C-1110 from the Wright Research and Development Center.

G.-W. Pan is with the Department of Electrical Engineering, University of Wisconsin-Milwaukee, WI 53201.

B. K. Gilbert is with the Special Purpose Development Group, Mayo Foundation, Department of Physiology and Biophysics, Rochester, MN 53905.

G. J. Wunsch is with the Department of Electrical and Computer Engineering University of Massachusetts, Amherst, MA 01002-9987.

IEEE Log Number 9202895.

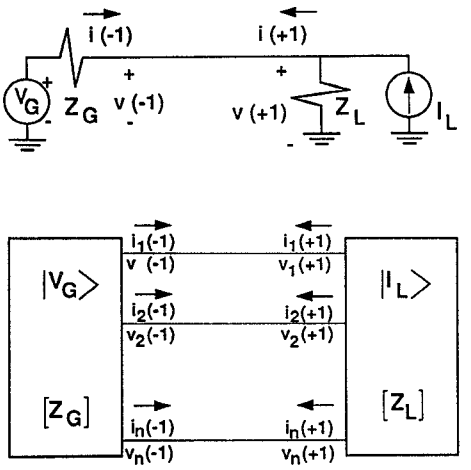

Fig. 1. Schematic Diagram of lossy nonuniform transmission line systems. Upper: Single transmission line system; Lower: multiple transmission line system.

frequency. The capacitance (electrostatic induction coefficients) and external inductance seem not to vary appreciably with frequency. We will, however, characterize all four parameters, i.e., capacitance, inductance, resistance and conductance, as functions of ω for maximum generality. Since the transmission line under consideration has variable geometry with respect to the distance coordinate, the quasistatic parameters will be functions of this distance parameter.

The pseudo-spatial method using Chebyshev coefficients was chosen to solve this problem. Chebyshev expansions are defined on the interval $x \in [-1, +1]$. However, transmission line problems are usually formulated in the interval $z \in [0, l]$, where l is the length of the line. Therefore, the linear transformation $x = (2z/l) - 1$ is performed before proceeding with the analysis. Note that the use of this transformation requires the values of the line parameters to be scaled by $l/2$.

We expand the (known) quasi-static parameters in a Chebyshev series. For example, the mutual inductance of the kth line on the jth line is $L^{(jk)}(x, \omega)$ and can be expanded as

$$L^{(jk)}(x, \omega) = \sum_{n=0}^{\infty}{}' l_n^{(jk)}(\omega)\, T_n(x) \tag{1}$$

where $T_n(x)$ is the Chebyshev polynomial of type 1 and order n, and Σ' is defined as

$$\sum_{n=0}^{\infty}{}' \Phi_n = \tfrac{1}{2}\Phi_0 + \Phi_1 + \Phi_2 + \cdots. \tag{2}$$

since $L^{(jk)}(x, \omega)$ can be determined from the geometry, the coefficients $l_n^{(jk)}(\omega)$ are given by

$$l_n^{(jk)}(\omega) = \int_{-1}^{+1} \frac{L^{(jk)}(x, \omega)\, T_n(x)}{\sqrt{1 - x^2}}\, dx. \tag{3}$$

The method used to calculate the parameters as functions of distance is to slice the line at certain points along its length. The parameters can be calculated by computer aided design tools, for instance, MagiCAD [6]–[9]. We can now define a piecewise linear function for the parameters. This function is then expanded by the above equation. Truncation of the series gives a polynomial with minimal maximum error for the number of terms chosen (this reduces the chance of strictly positive parameters becoming negative throughout any portion of the length of the line).

The telegraphist's equations are used to solve the system for $v(x, t)$ and $i(x, t)$ (specifically the near-end $v(-1, t)$ and far-end $v(+1, t)$ voltages. In the frequency domain the telegraphist's equations are

$$-\frac{dv_j(x, \omega)}{dx} = \sum_{k=1}^{N} (R^{(jk)}(x, \omega) + j\omega L^{(jk)})\, i_k(x, \omega) \tag{4}$$

$$-\frac{di_j(x, \omega)}{dx} = \sum_{k=1}^{N} (G^{(jk)}(x, \omega) + j\omega C^{(jk)})\, v_k(x, \omega). \tag{5}$$

2.1 Single Line Case

Rewriting these telegraphist's equations for a single line, with the line length normalized to the interval $x \in [-1, +1]$, we have

$$\frac{dv(x, \omega)}{dx} = -Z(x, \omega)\, i(x, \omega) \tag{6}$$

$$\frac{di(x, \omega)}{dx} - -Y(x, \omega)\, v(x, \omega) \tag{7}$$

where

$$Z(x, \omega) = R(x, \omega) + j\omega L(x, \omega) \tag{8}$$

$$Y(x, \omega) = G(x, \omega) + j\omega C(x, \omega). \tag{9}$$

The derivatives of voltage and current with respect to x are given by

$$\frac{dv(x, \omega)}{dx} = \sum_{n=0}^{N_C}{}' a_n(\omega)\, \frac{d}{dx}\,[T_n(x)] = \sum_{n=0}^{N_C}{}' a_n^*(\omega)\, T_n(x) \tag{10}$$

$$\frac{di(x, \omega)}{dx} = \sum_{n=0}^{N_C}{}' b_n(\omega)\, \frac{d}{dx}\,[T_n(x)] = \sum_{n=0}^{N_C}{}' b_n^*(\omega)\, T_n(x) \tag{11}$$

where the relation

$$a_n = \frac{1}{2n}\,(a_{n-1}^* - a_{n+1}^*) \tag{12}$$

holds for $n = 1, 2, \cdots$. The a_0 and b_0 terms are lost due to the differentiation. These terms are to be determined later according to the boundary equations of the problem. Now define the vectors $|a\rangle$, $|a^1\rangle$ and $|a^*\rangle$:

$$|a\rangle = [a_0 \quad a_1 \quad \cdots \quad a_{N_C}]^T \tag{13}$$

$$|a^1\rangle = [a_1 \quad a_2 \quad \cdots \quad a_{N_C+1}]^T \tag{14}$$

$$|a^*\rangle = [a_0^* \quad a_1^* \quad \cdots \quad a_{N_C}^*]^T. \tag{15}$$

We can now write:

$$|a^1\rangle = \boldsymbol{D}^C |a^*\rangle \tag{16}$$

and defining $|b\rangle$, $|b^1\rangle$ and $|b^*\rangle$, in a similar manner we can write:

$$|b^1\rangle = \boldsymbol{D}^C |b^*\rangle \tag{17}$$

where $\boldsymbol{D}^C$ is called the Chebyshev differentiation matrix and the entries of the ith row and jth column of this matrix are given by

$$D^C(i,j) = \begin{cases} \dfrac{1}{2i} & \text{for } i = j \\ -\dfrac{1}{2i} & \text{for } i = j-2;\ i,j = 1, 2, \cdots, N_C+1. \\ 0 & \text{otherwise} \end{cases} \tag{18}$$

The nonuniformity of the line parameters can be characterized by means of their expansion coefficients. Substituting the expansions developed above into the original equation, we have

$$\sum_{n=0}^{N_C}{}' a_n^*(\omega)\, T_n(x) = \left(-\sum_{n=0}^{N_C}{}' b_n(\omega)\, T_n(x)\right)\left(\sum_{k=0}^{N_C}{}' z_k(\omega)\, T_k(x)\right) = -\sum_{n=0}^{N_C}{}' \sum_{k=0}^{N_C}{}' b_n(\omega) z_k(\omega)\, T_n(x)\, T_k(x) \tag{19}$$

$$\sum_{n=0}^{N_C}{}' b_n^*(\omega)\, T_n(x) = \left(-\sum_{n=0}^{N_C}{}' a_n(\omega)\, T_n(x)\right)\left(\sum_{k=0}^{N_C}{}' y_k(\omega)\, T_k(x)\right) = -\sum_{n=0}^{N_C}{}' \sum_{k=0}^{N_C}{}' a_n(\omega) y_k(\omega)\, T_n(x)\, T_k(x). \tag{20}$$

Taking the Chebyshev inner product of both sides of these equations, and using the Chebyshev triple product, we arrive at

$$|a^*\rangle = \boldsymbol{X}_Z |b\rangle \tag{21}$$

$$|b^*\rangle = \boldsymbol{X}_Y |a\rangle \tag{22}$$

where the entries of the ith row and jth column (beginning with row and column number 0) of $\boldsymbol{X}_Z$ and $\boldsymbol{X}_Y$ are given by

$$X_Z(i,j) = \alpha_{ij}(Z_{i+j} + Z_{|i-j|}) \tag{23}$$

$$X_Y(i,j) = \alpha_{ij}(Y_{i+j} + Y_{|i-j|}) \tag{24}$$

for $i, j = 0, 1, 2, \cdots, N_C$ and

$$\alpha_{ij} = \begin{cases} -1/4 & \text{if } j = 0 \\ -1/2 & \text{otherwise.} \end{cases} \tag{25}$$

A pair of vectors that will be useful later are the row vectors of length $N_C + 1$, $\langle f_N|$ and $\langle f_F|$, defined as

$$\langle f_N| = [\tfrac{1}{2} \quad -1 \quad 1 \quad -1 \quad \cdots \quad (-1)^{N_C}]$$

$$\langle f_F| = [\tfrac{1}{2} \quad 1 \quad 1 \quad 1 \quad \cdots \quad 1]. \tag{26}$$

By using the identities $T_n(+1) = +1$ and $T_n(-1) = (-1)^n$ we can see that the near/far end voltages/currents can be written as

$$\langle f_N|\, a\rangle = v(-1) \tag{27}$$

$$\langle f_F|\, a\rangle = v(+1) \tag{28}$$

$$\langle f_N|\, b\rangle = i(-1) \tag{29}$$

and

$$\langle f_F|\, b\rangle = i(+1). \tag{30}$$

The series $\Sigma_n^{N_C+1} a_n T_n(x)$ should approximate the voltage $v(x)$ as well as $\Sigma_n^{N_C} a_n T_n(x)$ if N_C is chosen large enough (that is, $a_{N_C+1} \to 0$) so that at the far end

$$v(+1) = \frac{a_0}{2} + a_1 + a_2 + \cdots + a_{N_C+1} \tag{31}$$

or

$$a_{N_C+1} = -\frac{a_0}{2} - a_1 - a_2 - \cdots - a_{N_C} + v(+1) \tag{32}$$

allowing us to write in vector/matrix form

$$|a^1\rangle = \boldsymbol{Q}_F |a\rangle + v(+1)\,|e_F\rangle \tag{33}$$

where $\boldsymbol{Q}_F$ and $|e_F\rangle$ are defined as

$$\boldsymbol{Q}_F = \begin{bmatrix} 0 & 1 & 0 & \cdots & 0 \\ 0 & 0 & 1 & \cdots & 0 \\ \vdots & \vdots & \vdots & \ddots & \vdots \\ -\frac{1}{2} & -1 & -1 & \cdots & -1 \end{bmatrix} \tag{34}$$

$$|e_F\rangle = [0 \quad 0 \quad \cdots \quad 1]^T. \tag{35}$$

Similarly, at the near end of the line the current can be written as

$$|b^1\rangle = \boldsymbol{Q}_N |b\rangle + i(-1)\,|e_N\rangle \tag{36}$$

and $\boldsymbol{Q}_N$ and $|e_N\rangle$ are defined as

$$\boldsymbol{Q}_N = \begin{bmatrix} 0 & 1 & 0 & \cdots & 0 \\ 0 & 0 & 1 & \cdots & 0 \\ \vdots & \vdots & \vdots & \ddots & \vdots \\ \frac{1}{2}(-1)^{N_C} & -(-1)^{N_C} & (-1)^{N_C} & \cdots & 1 \end{bmatrix} \tag{37}$$

$$|e_N\rangle = [0 \quad 0 \quad \cdots \quad (-1)^{N_C+1}]^T. \tag{38}$$

Consider a line terminated at one end by a generator voltage in series with a generator (source) impedance, and at the other with a load impedance. The termination equations are then written as

$$V_G = Z_G i(-1) + v(-1) \tag{39}$$

$$v(+1) = Z_L i(+1) \tag{40}$$

Defining the column vectors $|W_{NF}\rangle$ and $|W_{FN}\rangle$:

$$|W_{NF}\rangle = \begin{bmatrix} v(-1) \\ i(+1) \end{bmatrix}$$

$$|W_{FN}\rangle = \begin{bmatrix} v(+1) \\ i(-1) \end{bmatrix} \tag{41}$$

we can write the termination equations in vector/matrix form as

$$|W_{NF}\rangle = \boldsymbol{Z}_T |W_{FN}\rangle + |U\rangle \tag{42}$$

where $\boldsymbol{Z}_T$ and $|U\rangle$ are given by

$$\boldsymbol{Z}_T = \begin{bmatrix} 0 & -Z_G \\ Z_L^{-1} & 0 \end{bmatrix} \tag{43}$$

and

$$|U\rangle = \begin{bmatrix} V_G \\ 0 \end{bmatrix}. \tag{44}$$

Combining (17), (22) and (36), we write

$$\boldsymbol{D}^C \boldsymbol{X}_Y |a\rangle = \boldsymbol{Q}_N |b\rangle + i(-1)|e_N\rangle. \tag{45}$$

Combining equations (16), (21) and (33), we write

$$\boldsymbol{D}^C \boldsymbol{X}_Z |b\rangle = \boldsymbol{Q}_F |a\rangle + v(+1)|e_F\rangle \tag{46}$$

In vector/matrix form, these equations become

$$\boldsymbol{X}_H |p\rangle = \boldsymbol{Q}_{NF} |p\rangle + \boldsymbol{E}_{NF} |W_{FN}\rangle \tag{47}$$

with the following definitions:

$$\boldsymbol{X}_H = \begin{bmatrix} \boldsymbol{D}^C \boldsymbol{X}_Y & 0 \\ \boldsymbol{0} & \boldsymbol{D}^C \boldsymbol{X}_Z \end{bmatrix} \tag{48}$$

$$|p\rangle = \begin{bmatrix} |a\rangle \\ |b\rangle \end{bmatrix} \tag{49}$$

$$\boldsymbol{Q}_{NF} = \begin{bmatrix} \boldsymbol{0} & \boldsymbol{Q}_N \\ \boldsymbol{Q}_F & \boldsymbol{0} \end{bmatrix} \tag{50}$$

$$\boldsymbol{E}_{NF} = \begin{bmatrix} |0\rangle & |e_N\rangle \\ |e_F\rangle & |0\rangle \end{bmatrix}. \tag{51}$$

Solving this equation, we have

$$|p\rangle = (\boldsymbol{X}_H - \boldsymbol{Q}_{NF})^{-1} \boldsymbol{E}_{NF} |W_{FN}\rangle \tag{52}$$

Defining $\boldsymbol{F}_{NF}$ to be

$$\boldsymbol{F}_{NF} = \begin{bmatrix} \langle f_N| & \langle 0| \\ \langle 0| & \langle f_F| \end{bmatrix} \tag{53}$$

we have

$$|W_{NF}\rangle = \boldsymbol{F}_{NF} |p\rangle \tag{54}$$

and now the general solution for the single line case can be written as

$$|p\rangle = (\boldsymbol{X}_H - \boldsymbol{Q}_{NF})^{-1} \boldsymbol{E}_{NF} \cdot \{\boldsymbol{F}_{NF}[\boldsymbol{X}_H - \boldsymbol{Q}_{NF}]^{-1} \boldsymbol{E}_{NF} - \boldsymbol{Z}_T\}^{-1} |U\rangle. \tag{55}$$

2.2 Multiple Coupled Lines

In practice, the important issues are crosstalk values between lines, the effect of multiple reflections (due to mismatching), their effects through coupling to the neighboring lines, and so on. These issues can be addressed through the analysis of multiple coupled tapered lines. The extension from the single line case to the multiple line case is straightforward (except for notation), and is derived in the appendix for the review of interested readers. In the following section, we will present a set of results from real world problems found in actual interconnect structures, using the equations derived in the appendix for the multiple tapered line case.

III. Numerical Examples

To illustrate the effectiveness of the frequency domain method described in this paper, three examples will be presented. In the first two, we will compare our results with data from the literature; the agreement of the results from this new method with the published data are quite impressive. The last example deals with tapered lossy and coupled lines, for which no comparison is as yet available.

Example 1—Tapered Lossless Coupled Lines: Fig. 2 depicts the geometry and terminations of the tapered lines discussed in [5], for which inductance and capacitance matrices, as a function of distance, were computed section by section using the Mayo MagiCAD computer aided design system. In Figs. 3U and 3L, waveforms at the near and far ends, for both the active and passive lines, are presented using a Chebyshev series containing eight terms, in the time and frequency domains respectively. It will be observed that the results of the time domain Chebyshev algorithm in Fig. 3U and the frequency domain Chebyshev algorithm in Fig. 3L agree extemely well. The execution times on a VAX-3500 for the two algorithms were 5.2 s and 5.6 s respectively. As the geometries become more complicated, the frequency domain method will be more efficient than the time domain approach.

Example 2—Uniform Lossy Coupled Lines: To test the ability of the new algorithm to handle frequency dependent parameters, we compared our results for "tapered" lines with zero tapering angle against the uniform line algorithm of Djordjevic [7] in Figs. 4U and 4L. The resistance matrix was assumed to vary in proportion to the square root of frequency (although a more complicated

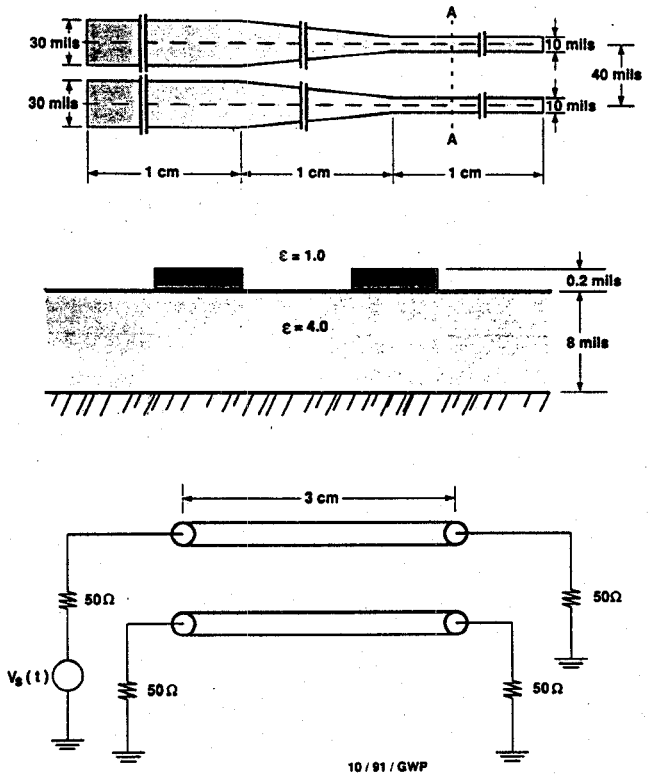

Fig. 2. Lossless tapered transission line structures typically found in printed circuit boards and multichip modules. Upper: top view; Middle: edge view; Lower: electrical equivalent line.

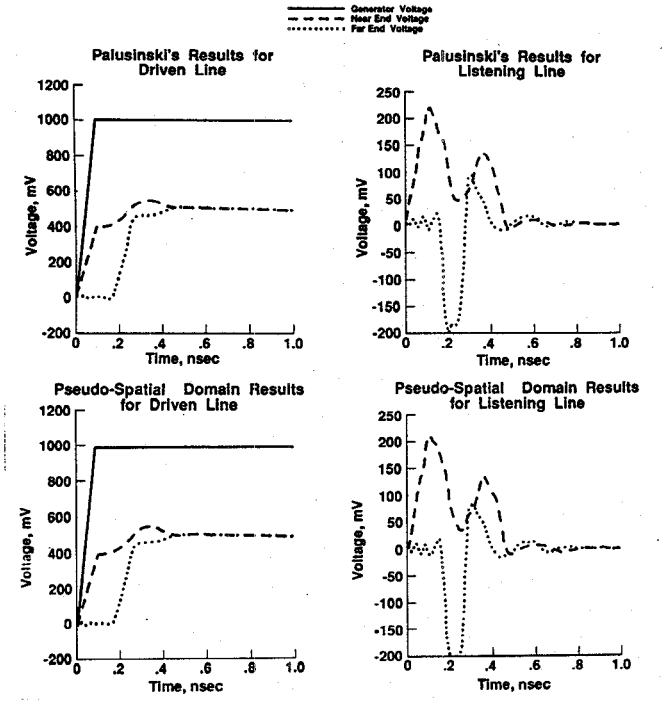

Fig. 3. Comparison of simulation results from Palusinski's method with results from pseudo-spatial domain tapered line algorithm of electrical response of two tapered lossless microstrip transmission lines. Upper: Palusinski's results; Lower: pseudo-spatial domain results.

function or even a lookup table can also be incorporated). Again, the agreement of the two methods was excellent.

Example 3—Tapered Lossy Coupled Lines: Two coupled lossy, nonuniform copper lines, with a total length of 5 cm, are presented in Fig. 5U; for comparison, the geometric equivalent "average" line pair, i.e., two uniform lines, is depicted in Fig. 5L. The conduction loss was not assumed to vary in proportion to the square root of frequency, because the dimension of the line cross section is of the same order as, or even smaller than, the skin depth (for a frequency component range of dc-3 GHz). Further, we have found that if we do assume that conduction loss varies in proportion to the square root of frequency, the resulting simulations exhibit a violation of causality. That is, the output waveforms at the far end of the line appear at the same instant as the input waveforms are applied to the near end of the line, which is physically impossible given that the length between the input and output ends of the interconnect was nonzero in the simulations. Instead, normalized frequencies [10] for each cross sectional slice along the length of the lines were calculated and the corresponding resistances as a function of frequency were obtained. Fig. 6U illustrates the waveforms of the driven and listening lines at both near and far ends. Fig. 6L shows waveforms of the same lines as in Fig. 6U, but the direction of the taper has been reversed (so that the waveform results will be different).

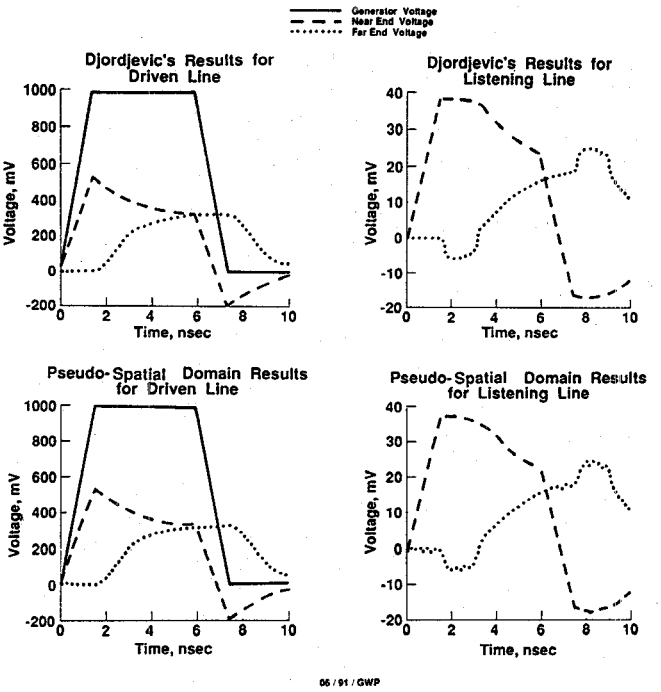

Fig. 4. Comparison of simulation results from Djordjevic's method and from pseudo-spatial domain tapered line algorithm of electrical response of two parallel uniform transmission lines. Upper: Djordjevic's results; Lower: pseudo-spatial domain results.

To compare the lossy case results with results from lossless lines of the same geometry and with lossy lines of uniform mean cross sections, two additional cases were simulated. In Fig. 7U we used the same line geometry as in Fig. 6U, but an infinite conductivity was assumed so that the lines are lossless (dielectric losses are assumed to be so small that they may be neglected). By comparing Fig. 6U with 7U, we find that the conduction loss causes

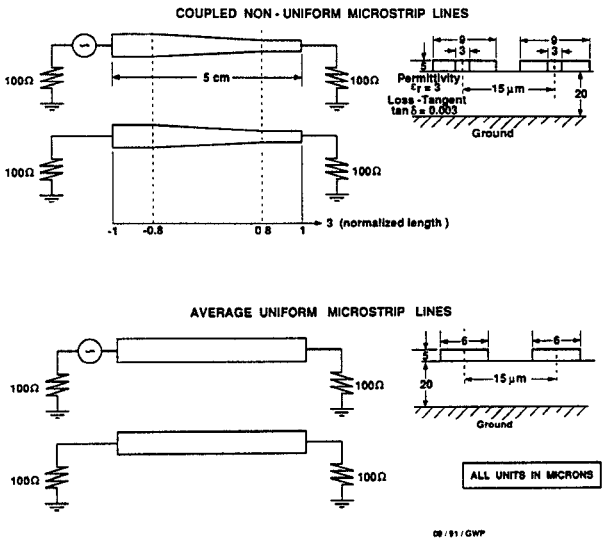

Fig. 5. Geometry and terminations of coupled nonuniform microstrip lines and their "average" uniform microstrip line equivalents. Upper: nonuniform line structure; Lower: average uniform line equivalents.

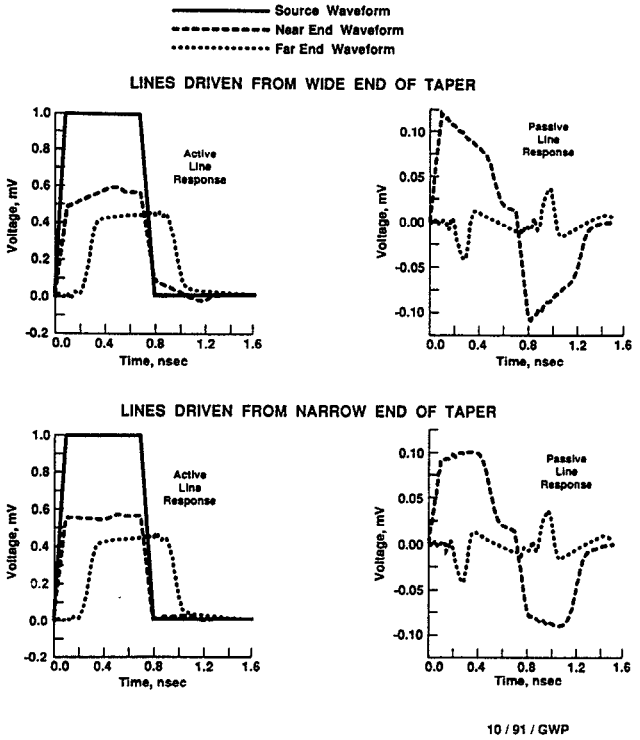

Fig. 6. Simulation results from pseudo-spatial domain tapered line algorithm of electrical response for lossy, tapered microstrip transmission lines driven from both wide and narrow ends.

the far-end waveform to be of smaller amplitude and smoother than that from the lossless line; meanwhile, the conduction loss causes the near-end waveform to exhibit a larger amplitude. This is because the characteristic impedance of the lossy line is greater than that of the lossless line, and therefore, by the voltage division rule, a greater fraction of the total voltage from the generator is delivered to the line.

It may be observed by comparing Figs. 7L and 6U that the nonuniformity makes the near-end waveform more uneven; note the larger "hump" and steeper slope which

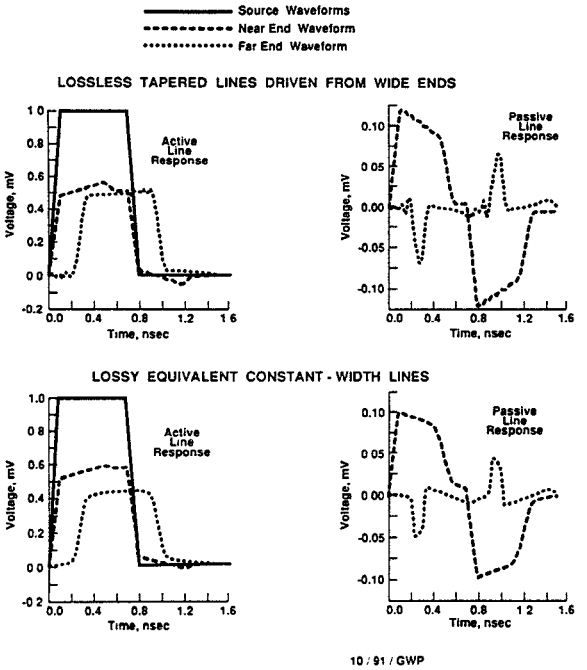

Fig. 7. Simulation results from pseudo-spatial domain tapered line algorithm of electrical response of lossless tapered microstrip transmission lines and lossy equivalent constant-width microstrip transmission lines.

are apparent on the "logic high" portion of the waveform. This is due to positive reflections caused by the gradually increasing impedance of the tapered line. However, by reversing the direction of the line taper, the corresponding "logic high" region of the waveform shown in Fig. 6L is flatter than is the case for the uniform lines, because the negative reflections of the gradually decreasing impedance partially cancel the rising voltage values in the logic high region of the uniform line; in the meantime, the near-end crosstalk voltage is also minimized. By changing the tapering angle and direction, the waveform can be well controlled. This ability to alter the conformation of the waveforms to any desired shape may find some useful applications in practice. In each of the cases discussed in Example 3, eight Chebyshev terms and 1024 FFT points were used; the execution time on a VAX-3500 was 37 s.

IV. Conclusions

In this paper, a technique has been described for the analysis of the wavefront propagation characteristics of multiple tapered stripline and microstrip lines used as interconnects in high speed, high density multichip digital circuits. The frequency domain method computes crosstalk and waveform distortions, and correctly accounts for conductor losses (as a function of frequency) and for varying conductor widths and spacing. The technique, referred to as the pseudo-spatial technique, utilizes the orthogonality of both Fourier transform and Chebyshev expansions to simplify the mathematical formulation. It turns out that the new algorithm solves uniform lines as a special case, almost as rapidly as do less general methods (modal analysis [7], for instance).

An improvement over the time domain approach was achieved by avoiding time stepping recursive computations and state matrix computations, thus improving numerical efficiency and stability. Frequency dependent phenomena, including skin effect, internal inductance and dielectric loss can also be addressed by this technique. The frequency domain algorithm is also easier to incorporate with other transmission line networking CAD packages, which themselves operate in the frequency domain. The pseudo-spatial method was derived under the quasi-TEM assumption, in that any dispersive effects caused by transverse current flows were ignored. However, within a frequency range of less than approximately 5 GHz, these derivations using the Quasi-TEM assumption appear to provide an excellent simulation of the performance of tapered lines, and great simplicity in both derivation and implementation.

Appendix
Derivation of Multiple Coupled Line Case

As an extension of the results derived in Section 2.1 for the single line case, we derive in this appendix the equations for the case of multiple coupled tapered lines. The voltage and current on the jth line of an N line system is given by the following equations:

$$\frac{dv_j}{dx} = -\sum_{k=1}^{N} Z^{(jk)}(x)\, i_k \tag{56}$$

$$\frac{di_j}{dx} = -\sum_{k=1}^{N} Y^{(jk)}(x)\, v_k \tag{57}$$

for any particular frequency. Here, $Z^{(jk)}(x)$ and $Y^{(jk)}(x)$ represent the self ($j = k$) and mutual impedances and admittances of the kth line on the jth line, which are given by

$$Z^{(jk)}(x) = R^{(jk)}(x) + j\omega L^{(jk)}(x) \tag{58}$$

$$Y^{(jk)}(x) = G^{(jk)}(x) + j\omega C^{(jk)}(x). \tag{59}$$

The Chebyshev expansions of voltage and current for the jth line are

$$v_j = \sum_{n=0}^{Nc}{}' a_n^{(j)} T_n(x) \tag{60}$$

$$i_j = \sum_{n=0}^{Nc}{}' b_n^{(j)} T_n(x). \tag{61}$$

The differentiation relation still holds, and can be written as

$$|a^{(j)1}\rangle = \boldsymbol{D}^C |a^{(j)*}\rangle \tag{62}$$

$$|b^{(j)1}\rangle = \boldsymbol{D}^C |b^{(j)*}\rangle \tag{63}$$

The entries of the nonuniformity matrices, $\boldsymbol{X}_Z^{(mn)}$ and $\boldsymbol{X}_Z^{(mn)}$ can be written as

$$X_Z^{(mn)}(i,j) = \alpha_{ij}[Z_{i+j}^{(mn)} + Z_{|i-j|}^{(mn)}] \tag{64}$$

$$X_Y^{(mn)}(i,j) = \alpha_{ij}[Y_{i+j}^{(mn)} + Y_{|i-j|}^{(mn)}] \tag{65}$$

where α_{ij} is given by (25). For the jth line, then

$$|a^{(j)*}\rangle = \boldsymbol{X}_Z^{(j1)}|b^{(1)}\rangle + \boldsymbol{X}_Z^{(j2)}|b^{(2)}\rangle + \cdots + \boldsymbol{X}_Z^{(jN)}|b^{(N)}\rangle \tag{66}$$

$$|b^{(j)*}\rangle = \boldsymbol{X}_Y^{(j1)}|a^{(1)}\rangle + \boldsymbol{X}_Y^{(j2)}|a^{(2)}\rangle + \cdots + \boldsymbol{X}_Y^{(jN)}|a^{(N)}\rangle. \tag{67}$$

Now if we define the following $N \times (N_C + 1)$ length column vectors, the pertinent equations can be written in more compact form as

$$|A^*\rangle = \begin{bmatrix} |a^{(1)*}\rangle \\ |a^{(2)*}\rangle \\ \vdots \\ |a^{(N)*}\rangle \end{bmatrix}; \quad |B^*\rangle = \begin{bmatrix} |b^{(1)*}\rangle \\ |b^{(2)*}\rangle \\ \vdots \\ |b^{(N)*}\rangle \end{bmatrix} \tag{68}$$

$$|A\rangle = \begin{bmatrix} |a^{(1)}\rangle \\ |a^{(2)}\rangle \\ \vdots \\ |a^{(N)}\rangle \end{bmatrix}; \quad |B\rangle = \begin{bmatrix} |b^{(1)}\rangle \\ |b^{(2)}\rangle \\ \vdots \\ |b^{(N)}\rangle \end{bmatrix} \tag{69}$$

$$|A^1\rangle = \begin{bmatrix} |a^{(1)^1}\rangle \\ |a^{(2)^1}\rangle \\ \vdots \\ |a^{(N)^1}\rangle \end{bmatrix}; \quad |B^1\rangle = \begin{bmatrix} |b^{(1)^1}\rangle \\ |b^{(2)^1}\rangle \\ \vdots \\ |b^{(N)^1}\rangle \end{bmatrix}. \tag{70}$$

Defining $\boldsymbol{X}_Z$ and $\boldsymbol{X}_Y$ to be

$$\boldsymbol{X}_Z = \begin{bmatrix} \boldsymbol{X}_Z^{(11)} & \boldsymbol{X}_Z^{(12)} & \cdots & \boldsymbol{X}_Z^{(1N)} \\ \boldsymbol{X}_Z^{(21)} & \boldsymbol{X}_Z^{(22)} & \cdots & \boldsymbol{X}_Z^{(2N)} \\ \vdots & \vdots & \ddots & \vdots \\ \boldsymbol{X}_Z^{(N1)} & \boldsymbol{X}_Z^{(N2)} & \cdots & \boldsymbol{X}_Z^{(NN)} \end{bmatrix} \tag{71}$$

$$\boldsymbol{X}_Y = \begin{bmatrix} \boldsymbol{X}_Y^{(11)} & \boldsymbol{X}_Y^{(12)} & \cdots & \boldsymbol{X}^{(1N)} \\ \boldsymbol{X}_Y^{(21)} & \boldsymbol{X}_Y^{(22)} & \cdots & \boldsymbol{X}^{(2N)} \\ \vdots & \vdots & \ddots & \vdots \\ \boldsymbol{X}_Y^{(N1)} & \boldsymbol{X}_Y^{(N2)} & \cdots & \boldsymbol{X}_Y^{(NN)} \end{bmatrix} \tag{72}$$

we can write

$$|A^*\rangle = \boldsymbol{X}_Z|B\rangle \tag{73}$$

and

$$|B^*\rangle = \boldsymbol{X}_Y|A\rangle. \tag{74}$$

With $\boldsymbol{D}_D^C$ defined as the block diagonal of $\boldsymbol{D}^C$ we can write the differentiation matrix equation as

$$|A^1\rangle = \boldsymbol{D}_D^C|A^*\rangle \tag{75}$$

$$|B^1\rangle = \boldsymbol{D}_D^C|B^*\rangle. \tag{76}$$

The boundary condition relations for each line still hold, in the form of

$$|a^{(j)1}\rangle = \boldsymbol{Q}_F|a^{(j)}\rangle + v_j(+1)|e_f\rangle \tag{77}$$

$$|b^{(j)1}\rangle = \boldsymbol{Q}_N|b^{(j)}\rangle + i_j(-1)|e_N\rangle \tag{78}$$

so that if we define $\boldsymbol{Q}_{FD}$, $\boldsymbol{E}_{FD}$, $\boldsymbol{Q}_{ND}$, $\boldsymbol{E}_{ND}$ to be the block diagonal matrices/vectors of $\boldsymbol{Q}_F$, $\boldsymbol{E}_F$, $\boldsymbol{Q}_N$, $\boldsymbol{E}_N$, respectively, then the boundary condition relations are

$$|A^1\rangle = \boldsymbol{Q}_{FD}|A\rangle + \boldsymbol{E}_{FD}|v(+1)\rangle \tag{79}$$

$$|B^1\rangle = \boldsymbol{Q}_{ND}|B\rangle + \boldsymbol{E}_{ND}|i(-1)\rangle \tag{80}$$

so that we can now combine (76), (74) and (80) into

$$\boldsymbol{D}_D^C\boldsymbol{X}_Y|A\rangle = \boldsymbol{Q}_{ND}|B\rangle + \boldsymbol{E}_{ND}|i(-1)\rangle. \tag{81}$$

and we can also combine (75), (73) and (79) to form

$$\boldsymbol{D}_D^C\boldsymbol{X}_Z|B\rangle = \boldsymbol{Q}_{FD}|A\rangle + \boldsymbol{E}_{FD}|v(+1)\rangle \tag{82}$$

so that in turn, we can define

$$|P\rangle = \begin{bmatrix} |A\rangle \\ |B\rangle \end{bmatrix} \tag{83}$$

$$\boldsymbol{X}_H = \begin{bmatrix} \boldsymbol{D}_D^C\boldsymbol{X}_Y & \boldsymbol{0} \\ \boldsymbol{0} & \boldsymbol{D}_D^C\boldsymbol{X}_Z \end{bmatrix} \tag{84}$$

$$\boldsymbol{Q}_{NF} = \begin{bmatrix} \boldsymbol{0} & \boldsymbol{Q}_{ND} \\ \boldsymbol{Q}_{FD} & \boldsymbol{0} \end{bmatrix} \tag{85}$$

$$\boldsymbol{E}_{NF} = \begin{bmatrix} \boldsymbol{0} & \boldsymbol{E}_{ND} \\ \boldsymbol{E}_{FD} & \boldsymbol{0} \end{bmatrix} \tag{86}$$

and write

$$\boldsymbol{X}_H|P\rangle = \boldsymbol{Q}_{NF}|P\rangle + \boldsymbol{E}_{NF}|\boldsymbol{W}_{FN}\rangle \tag{87}$$

Again, if we define $\boldsymbol{F}_{ND}$ and $\boldsymbol{F}_{FD}$ to be the block diagonal of the vectors $\langle f_N|$ and $\langle f_F|$ respectively, and define

$$\boldsymbol{F}_{NF} = \begin{bmatrix} \boldsymbol{F}_{ND} & \boldsymbol{0} \\ \boldsymbol{0} & \boldsymbol{F}_{FD} \end{bmatrix} \tag{88}$$

we can then write

$$\boldsymbol{F}_{NF}|P\rangle = |W_{NF}\rangle. \tag{89}$$

The terminations on each line are described for the jth line, by the equations

$$V_G^{(j)}(\omega) = Z_G^{(j)}i_j(-1) + v_j(-1) \tag{90}$$

$$i_j(+1) = \frac{v_j(+1)}{Z_L^{(j)}} + I_L^{(j)}(\omega). \tag{91}$$

Using the following definitions to simplify notation:

$$\boldsymbol{Z}_G = \begin{bmatrix} \boldsymbol{Z}_G^{(1)} & \boldsymbol{0} & \cdots & \boldsymbol{0} \\ 0 & \boldsymbol{Z}_G^{(2)} & \cdots & \boldsymbol{0} \\ \vdots & \vdots & \ddots & \vdots \\ \boldsymbol{0} & \boldsymbol{0} & \cdots & \boldsymbol{Z}_G^{(N)} \end{bmatrix} \tag{92}$$

$$\boldsymbol{Z}_L = \begin{bmatrix} \boldsymbol{Z}_L^{(1)} & \boldsymbol{0} & \cdots & \boldsymbol{0} \\ \boldsymbol{0} & \boldsymbol{Z}_L^{2} & \cdots & \boldsymbol{0} \\ \vdots & \vdots & \ddots & \vdots \\ \boldsymbol{0} & \boldsymbol{0} & \cdots & \boldsymbol{Z}_L^{(N)} \end{bmatrix} \tag{93}$$

$$\boldsymbol{Z}_T = \begin{bmatrix} \boldsymbol{0} & -\boldsymbol{Z}_G \\ \boldsymbol{Z}_L^{-1} & \boldsymbol{0} \end{bmatrix} \tag{94}$$

$$|v(\pm 1)\rangle = \begin{bmatrix} |v_1(\pm 1)\rangle \\ |v_2(\pm 1)\rangle \\ \vdots \\ |v_N(\pm 1)\rangle \end{bmatrix} \tag{95}$$

$$|i(\pm 1)\rangle = \begin{bmatrix} |i_1(\pm 1)\rangle \\ |i_2(\pm 1)\rangle \\ \vdots \\ |i_N(\pm 1)\rangle \end{bmatrix} \tag{96}$$

$$|W_{NF}\rangle = \begin{bmatrix} |v(-1)\rangle \\ |i(+1)\rangle \end{bmatrix} \tag{97}$$

$$|W_{FN}\rangle = \begin{bmatrix} |v(+1)\rangle \\ |i(-1)\rangle \end{bmatrix} \tag{98}$$

$$|V_G\rangle = \begin{bmatrix} |V_G^{(1)}\rangle \\ |V_G^{(2)}\rangle \\ \vdots \\ |V_G^{(N)}\rangle \end{bmatrix} \tag{99}$$

$$|I_L\rangle = \begin{bmatrix} |I_L^{(1)}\rangle \\ |I_L^{(2)}\rangle \\ \vdots \\ |I_L^{(N)}\rangle \end{bmatrix} \tag{100}$$

$$|U\rangle = \begin{bmatrix} |V_G\rangle \\ |I_L\rangle \end{bmatrix}. \tag{101}$$

This notation allows us to write

$$|W_{NF}\rangle = \boldsymbol{Z}_T|\boldsymbol{W}_{FN}\rangle + |U\rangle. \tag{102}$$

The solution, after algebraic manipulations, turns out to be

$$|P\rangle = (\boldsymbol{X}_H - \boldsymbol{Q}_{NF})^{-1}\boldsymbol{E}_{NF} \cdot \{\boldsymbol{F}_{NF}(\boldsymbol{X}_H - \boldsymbol{Q}_{NF})^{-1}\boldsymbol{E}_{NF} - \boldsymbol{Z}_T\}^{-1}|U\rangle. \tag{103}$$

Acknowledgment

The authors wish to thank S. Roosild and A. Prabhakar, DARPA/MTO, and J. Murphy, DARPA/ESTO, N. Ortwein, NOSC Code 80, and A. Tewksbury,

WR/ELEL, for support and helpful discussions; and E. Doherty, T. Funk, and S. Richardson for assistance in preparation of text and figures.

REFERENCES

[1] Q. Gu, J. Kong, and Y. Yang, "Time domain analysis of nonuniformly coupled line systems," *J. Electromagnetic Waves and Applications*, vol. 1, no. 2, pp. 109–132, 1987.

[2] Y. Yang, J. Kong, and Q. Gu, "Time-domain perturbational analysis of nonuniform coupled transmission lines," *IEEE Trans. Microwave Theory Tech.*, vol. MTT-33, pp. 1120–1130, Nov. 1985.

[3] P. Pramanick and P. Bhartia, "A generalized theory of tapered transmission line matching transformers and asymmetric couplers supporting non-TEM modes," *IEEE Trans. Microwave Theory Tech.*, vol. 37, no. 8, pp. 1184–1191, Aug. 1989.

[4] M. Mehalic and R. Mittra, "Investigation of tapered multiple microstrip lines for VLSI circuits," *IEEE Trans. Microwave Theory Tech.*, vol. 38, no. 11, pp. 1559–1566, Nov. 1990.

[5] O. A. Palusinski and A. Lee, "Analysis of Transients in Nonuniform and Uniform Multiconductor Transmission Lines," *IEEE Trans. Microwave Theory Tech.*, vol. 37, no. 1, pp. 127–138, Jan. 1989.

[6] B. Gilbert and G. Pan, "The application of gallium arsenide integrated circuit technology to design and fabrication of future generation digital signal processors: promises and problems," *Proc. IEEE*, vol. 76, no. 7, pp. 816–834, July 1988.

[7] A. Djordjevic and T. Sarkar, "Analysis of time response of lossy multiconductor transmission line networks," *IEEE Trans. Microwave Theory Tech.*, vol. MTT-35, no. 10, pp. 898–908, Oct. 1987.

[8] G. Pan, K. Olson, and B. Gilbert, "Improved algorithmic methods for the prediction of wavefront propagation behavior in multiconductor transmission lines for high frequency digital signal processors," *IEEE Trans. Computer-Aided Design*, vol. 8, no. 6, pp. 608–621, June 1989.

[9] G. Pan, K. Olson, and B. Gilbert, "Frequency-domain solution for coupled striplines with crossing strips," *IEEE Trans. Microwave Theory Tech.*, vol. 39, pp. 1013–1017, June 1991.

[10] R. Faraji-Dana and Y. Chow, "Edge condition of the field and ac resistance of a rectangular strip conductor," *Proc. IEEE*, vol. 137, pt. H, no. 2, pp. 133–140, Apr. 1990.

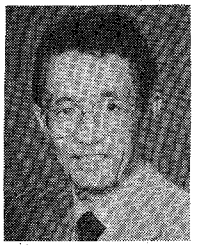

Guang-Wen Pan (S'81–83–M'84) attended Peking Institute of Petroleum Technology from 1962 through 1967, receiving a B.E. degree in Mechanical Engineering.

He then worked in machine design as an associate engineer for three years. From 1970 to 1978, he was employed at the Institute of Development and Research in China as an Electrical Engineer, responsible for design of pulse width modulation electronics and digital remote fire control systems used in petroleum seismic exploration. From 1978 to 1980 he attended graduate school at University of Science and Technology of China in Peking, majoring in electrical engineering. Dr. Pan came to the United States in 1980 as a research assistant in the Remote Sensing Laboratory, University of Kansas. In 1982, he earned an M.S., in Electrical Engineering, with emphasis on Telecommunication, Information Theory, Digital Radar Image Processing and Pattern Recognition. Beginning in 1982, he began work on theoretical modeling of radar bistatic scattering from randomly rough surfaces and theoretical work in the electromagnetics field. From September 1984 to May 1985, he was a Post Doctoral Fellow at the University of Texas, engaged in a project on Computer Aided Design of Airborne Antenna/Radome Systems. He joined the Mayo Foundation Special Purpose Processor Development Group in 1985, where he was engaged in the theoretical modeling of the electromagnetic behavior of VLSI/LSI integrated circuits, electronic circuit boards, and high density substrates. In 1986 he became an Associate Professor in the Department of Electrical Engineering, South Dakota State University, and in 1988 he joined the Department of Electrical Engineering at the University of Wisconsin, Milwaukee, also as an Associate Professor. His research interests continue to be in the mathematical modeling of the electromagnetic environment of high clock rate signal processors.

Gregory J. Wunsch received his B.S. degree in engineering from the University of Wisconsin-Milwaukee in 1983. From 1984 to 1988 he performed systems engineering work at the Boeing Company in Wichita, KS. He was employed as a research assistant from 1988 to 1991 at the University of Wisconsin-Milwaukee, where he received the M.S.E.E. degree in 1991. During this time he conducted research in association with the Mayo Foundation in Rochester, MN, where he held a research associate position in the summer of 1989.

Currently he is pursuing his Ph.D. at the University of Massachusetts at Amherst. His research interests currently include wave propagation, microelectronics packaging and efficient computation of solutions to the wave equation. He is a member of Tau Beta Pi.

Barry K. Gilbert (S'62–M'70–SM'87) received the B.S. degree in electrical engineering from Purdue University, Lafayette, IN, in 1965, and the Ph.D. degree in physiology and biophysics with minors in applied mathematics and electrical engineering, from the University of Minnesota, Minneapolis, in 1972.

He is presently a Staff Scientist and Professor in the Department of Physiology and Biophysics, Mayo Foundation, Rochester, MN. His research interests include the design of special-purpose processors for high-speed signal processing, and the development of advanced integrated circuit and electronic packaging technologies to support real-time signal processing of extremely wideband data. He has worked on a variety of projects, including the development in the mid 1970s of a very wideband special-purpose digital data handling and array processing computer fabricated entirely with subnanosecond emitter coupled logic, and a special-purpose multiple instruction, multiple data (MIMD) processor capable of operating with up to 30 coprocesors under parallel microcode control in the late 1970s. More than 25 digital Gallium Arsenide (GaAs) chips have been designed in his laboratory during the past decade, with several industrial collaborations under way to insert GaAs chips into existing signal processors. He is currently responsible for the development of CAD tools at the system and integrated circuit levels, as well as high density electronic packaging technologies, to allow the fabrication of signal processing modules operating at GHz clock rates using GaAs digital integrated circuits and multichip modules.